Renewable Energy 170 (2021) 1228–1244

Contents lists available at ScienceDirect

Renewable Energy

journal homepage: www.elsevier.com/locate/renene

Experimental investigation and analytical modelling of active yaw control for wind farm power optimization

Haohua Zong*, Fernando Porté-Agel

Wind Engineering and Renewable Energy Laboratory (WIRE), École Polytechnique Fédérale de Lausanne (EPFL), 1015, Lausanne, Switzerland

ARTICLE INFO

Article history:
Received 4 November 2020
Received in revised form
20 January 2021
Accepted 9 February 2021
Available online 13 February 2021

Keywords:
wind Farm
Power optimization
Active yaw control
Experiment
Analytical model

ABSTRACT

In this study, the physics and effectiveness of active yaw control under various wind conditions are investigated systematically, based on wind tunnel experiments and a new analytical wind farm model. The power and wake velocity measurements of a three-row miniature wind farm reveal that the peak power gain (18%) is reached in partial-wake conditions, when the wind direction is misaligned with the turbine column by 2–4°. In contrast, the power gain in the full-wake condition (5.4%) is a local minimum. For a single-column wind farm, the optimal yaw angle distribution always exhibits a decreasing trend from upstream to downstream, which can be associated with the secondary wake steering effect. Analytical model predicts that with increasing number of rows, both the peak power gain and the leading-turbine yaw angle increase asymptotically. The maximum value of the yaw angle is mainly determined by the cosine exponent of the thrust coefficient (p). With a typical value of $p = 1.8$, the maximum yaw angle value is approximately 30°. Turbulence intensity and streamwise spacing have similar effects on active yaw control. When these two parameters increase, the relative power gain decreases monotonically.

1. Introduction

For large wind farms consisting of dozens of wind turbines arranged closely in an array, the power losses resulting from inevitable wake interactions are significant, reaching up to 30–40% when the wind direction is aligned with turbine rows or columns [1,2]. To mitigate the wake-induced power losses, several wake redirection strategies have been proposed, including tilt angle adjustment, individual blade pitch control, and active yaw control (AYC). Tilt angle adjustment, although capable of elevating the vertical wake centre by approximately 0.2D (D denotes the rotor diameter), is not a controllable feature for utility-scale wind turbines [3]. Individual blade pitch control is easy to implement but less effective in mitigating wake effects. Moreover, it induces a substantial increase in the blade loading (> 100%), which adversely affects the life span of the major turbine components [3,4]. As a comparison, AYC not only induces appreciable wake deflections as large as 0.6D [5] but also has less impacts on the structural loads [6], thus gradually recognised as the most promising wake redirection strategy. Actually, several of the recent tests in commercial wind farms have already confirmed the effectiveness of AYC in power optimization [7–9].

Pivoting around how much power can be gained by AYC and what is the optimal yaw angle distribution, extensive studies have been carried out, involving mainly wind tunnel experiments and analytical model developments. The earliest experimental study of AYC is traced back to Ref. [10]; where an imaginary pentagon wind farm is considered. Due to the special layout, the wake interaction only occurs between two turbines, which allows the total power production to be derived from the power and wake velocity measurements of a stand-alone yawed wind turbine. As a result, turbine spacing (S_x) and the cosine exponent of the power coefficient (q) are identified as the two factors that significantly affect the power gain in AYC. For a typical range of $3D \leq S_x \leq 5D$ and $2 \leq q \leq 3$, the relative power gain averaged over all wind directions is 1.5–3%.

In [11,12]; two miniature wind turbines aligned in the streamwise direction are set up in the wind tunnel, and the effectiveness of AYC is validated by direct power measurements. Due to the different turbine spacing (3D vs. 2D) and incoming flow type (laminar vs. turbulent), the peak power gain achieved in these studies differs by a factor of two, being 12% and 6% respectively. Particularly [12], noticed that when the hub-height turbulence level reaches 18%, no power

* Corresponding author.
E-mail address: Haohua_Zong@126.com (H. Zong).

https://doi.org/10.1016/j.renene.2021.02.059
0960-1481/

improvement can be obtained by active yawing any more. Recently [13], applied AYC to a column of up to five miniature wind turbines. These turbines are spaced uniformly at 5D in the streamwise direction and submerged in a turbulent boundary layer developed naturally on the wind-tunnel wall (hub-height turbulence level: 6.5%). As a result, the relative power gain increases linearly with the number of rows, reaching 17% for five rows. The optimal yaw angle distribution is demonstrated to be a decreasing trend from upstream to downstream, with a maximum value of 30°.

Although the results obtained in wind tunnel experiments are encouraging, the two fundamental questions proposed earlier on (power gain and optimal yaw angle) remain unaddressed. To instruct the practical implementation of active yaw control in wind farms, computationally-cheap analytical models are highly demanded. Currently, two such models have been developed. In the one proposed by Ref. [14]; the streamwise variation of the peak wake velocity deficit is given by the Jensen-Park wake model [15], and the lateral wake deflection caused by yaw is integrated from the wake skew angle [16]. Applying this model to different sizes of wind farms, the authors concluded that the relative power gain from AYC increases monotonically with the number of wind turbines, consistent with the trends obtained in Ref. [13]. However, the maximum power gain is predicted to be achieved in the full-wake condition, which severely goes against the experimental results shown in Refs. [4,10]. Furthermore, it is also abnormal that, in their results, the optimal yaw angle of a wind turbine located in the centre is always the same as that in the front row (25°).

In [17]; the original top-hat wake model from Ref. [15] is modified by separately considering the wake expansion in three zones, and a similar parametric model for active yaw control (FLORIS) as that proposed by Ref. [14] is derived. When this model is applied to a three-row wind farm, a relative power gain of up to 13% is achieved at a turbulence intensity of 6%, which is close to the experimental value reported by Ref. [13]. Nevertheless, FLORIS predicts a maximum yaw angle of 40° at the second turbine row, which contradicts the decreasing trend of the optimal yaw angle distribution observed in experiments. Recently [18,19], derived a reduced-order wake model capable of capturing the secondary wake steering effect and the curled wake profile. They tested the performance of this model on a one-column wind farm, and found that the prediction accuracy of the optimal yaw angle distribution is noticeably improved with respect to FLORIS [19]. However, it has to be pointed out that the time this reduced-order model takes to compute the wind farm wake flow is three orders of magnitudes higher than the analytical models, i.e. several minutes for a wind farm with tens of wind turbines, thus inappropriate for parametric studies and online power optimization purposes.

In this study, wind tunnel experiments and analytical models are effectively combined to address the issue (i.e. accurate prediction of the relative power gain and optimal yaw angle distribution), hindering the practical implementation of AYC. In the experimental part, a three-row miniature wind farm is constructed, and the effectiveness of AYC at different wake conditions is investigated by power and wake velocity measurements. Details of the equipment and test schemes are described in Section 2. The trends of the measured wind farm efficiency and optimal yaw angle distribution are interpreted in section 3. Based on the physics learnt from experiments, a new analytical wind farm model is developed in section 4, which incorporates the recent progress in yawed wind turbine wakes and wake superposition principles. With this analytical model, a systematic study of the effectiveness of AYC is pursued (section 5), covering the influence of the number of rows/columns, turbulence intensity and streamwise spacing. Subsequently, the proposed model is applied to the Horns-Rev wind farm, and the corresponding results are presented in section 6. Section 7 concludes this study with a short summary.

2. Experiments setup

The experiments are carried out in the boundary layer wind tunnel at the WIRE laboratory of EPFL. This wind tunnel is a low-speed closed-loop wind tunnel, with a maximum free-stream velocity of 30 m/s and a typical turbulence level of 0.5%. The boundary layer originating from the contraction part develops naturally on the bottom wall of the test section under approximately zero pressure gradient. The length, width and height of the test section are 28 m, 2.6 m and 2 m, respectively. At 20 m downstream of the leading edge of the test section, a model wind farm consisting of three miniature wind turbines (WIRE-01, originally designed by Ref. [20] is constructed, as shown in Fig. 1. The rotor diameter and hub height of the WIRE-01 turbine are $D = 0.15$ m and $Z_h = 0.125$ m, respectively. The streamwise spacing between neighbouring wind turbines is fixed to five rotor diameters, i.e. $S_x = 5D$, and the spanwise spacing between adjacent wind turbines (S_y) can be adjusted to create either full-wake or partial-wake conditions. A coordinate system is established at the centreline of the test section, with its origin aligned with the tower of WT_1. The $x-$, $y-$, and $z-$ axes follow the streamwise, spanwise and wall-normal directions, respectively. For the purpose of this study, the time-averaged wind speed at the hub height (denoted as U_h) and the corresponding turbulence intensity are kept at 4.9 m/s and 7.1%. The boundary layer thickness at the wind farm inlet is approximately 0.3 m .

Seven different wake conditions are selected to test the feasibility of active yaw control, with the spanwise spacing between adjacent wind turbines ranging from $-1D$ to $1D$ in a step of $D/3$. In each wake condition, to search for the optimal yaw angle combination that leads to the maximum power production, the yaw angles of WT_1 and WT_2 (denoted as β_1 and β_2) are swept discretely from −40 to 40° in a step of either 5 or 10°, while the yaw angle of WT_3 is always kept at zero. The procedure of power measurements follows that detailed in Ref. [20]. Specifically, every time the yaw angle of WT_i is adjusted, the free rotation speed is measured in-situ, and the optimal rotation speed is interpolated from a pre-calibrated table. Once all the wind turbines are set, the output currents of the generators are recorded by a data acquisition board (National Instruments, PXIe-6358) for a duration of 180 s, at a sampling rate of 1 kHz. Based on the measured output current and rotation speed, the mechanical power extracted from the wind by each wind turbine (referred to as the mean power production hereinafter) can be calculated. The power measurement uncertainty evaluated from the standard deviation and the effective number of samples is less than 0.4% [21].

To reveal the physics of wake deflection, a high-resolution particle imaging velocimetry (PIV) system is deployed to measure the wake velocity fields at the hub level (i.e. $z = Z_h$). For each of the seven wake conditions, several yaw angle combinations are selected to execute PIV measurements, including but not limited to the baseline case of $\beta_1 = \beta_2 = 0$, and the optimal case where the power production is maximized. The PIV system consists of a camera (LaVision-sCMOS, sensor size 2560 × 2160 pixels), a double-pulse Nd:YAG laser (Litron, Nano TRL 425-10), and a programmable timing unit (LaVision, PTU-v9). The laser beam emitted from the laser head is shaped into a thin sheet parallel to the wall, by a combination of spherical and cylindrical lenses. The thickness of the laser sheet is adjusted to be 5 mm, as a compromise between the velocity measurement certainty and the spatial resolution. Olive oil particles of several microns in diameter are generated by an array of atomizers and released near the leading-edge of the test section to trace the flow. An objective of 50 mm in focal length is

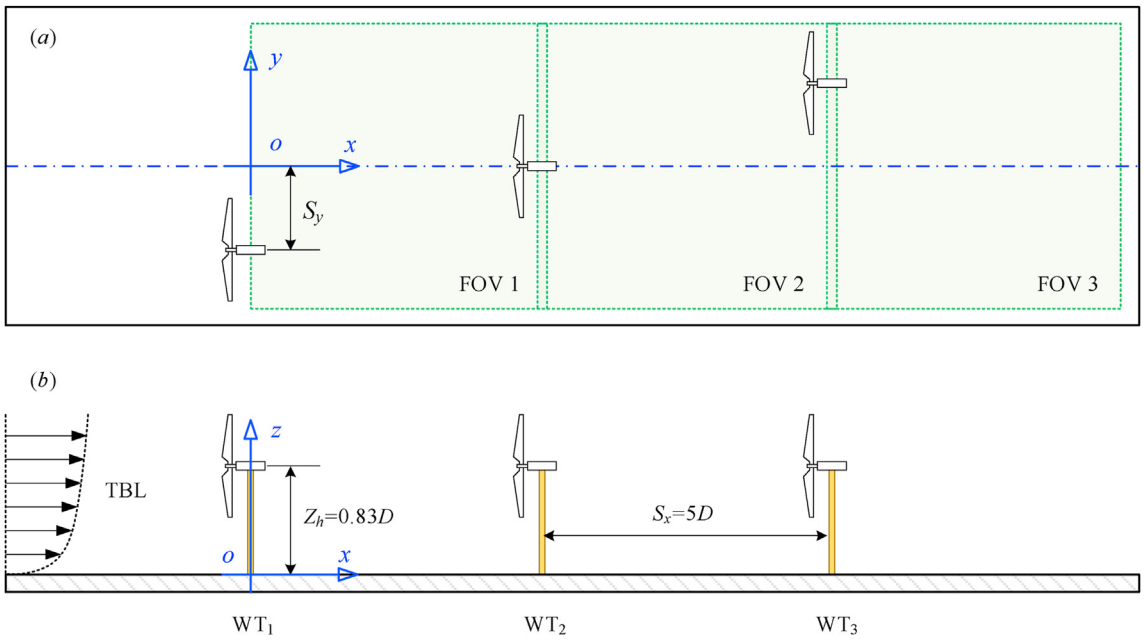

Fig. 1. Sketch of the model wind farm (not to scale): (*a*) top view, and (*b*) side view. The green rectangles in the top view indicate the field of views (FOVs) in PIV measurements.

fitted in front of the camera, resulting in a field of view (FOV) of approximately $5D \times 4.2D$. In order to capture the entire wake evolution in the model wind farm, the camera and laser optics are mounted on a traversing stage, and three sets of FOVs are arranged in the streamwise direction, covering an area of $15D \times 4D$, as shown in Fig. 1. For each FOV, 500 image pairs are acquired to get statistically converged mean velocity fields and turbulent quantities. During the post-processing of these images, the size and overlapping ratio of the interrogation window in the final pass of cross-correlation are selected as 16×16 and 75%, respectively, leading to a spatial resolution of 0.8 vector/mm.

In this study, the finite sample size and the peak locking error are identified as the two main sources of velocity measurement uncertainty. Following the approach described by Ref. [22]; the total measurement error for the time-averaged streamwise velocity and the kinetic energy are determined as 1.5% and 6.3%, respectively.

3. Experimental results and analysis

Prior to the presentation of experimental results, it is necessary to make a convention on the symbol usage. U and V are the time-averaged velocity in the streamwise and spanwise directions, respectively; β denotes the yaw angle; P_i, C_p^i, and C_t^i are the power production, power coefficient and thrust coefficient of the ith turbine ($i = 1, 2, \ldots N$), respectively; η is the overall wind farm efficiency defined as follows,

$$\eta = \frac{1}{NP_0}\sum_i P_i \tag{1}$$

where N denotes the number of wind turbines in the wind farm; P_0 is the power production of a stand-alone wind turbine. Other symbols will be introduced during their first occurrence

3.1. Full-wake condition

Under the full-wake condition, the relative variation of the wind farm efficiency (denoted as $\delta\eta$) is plotted in Fig. 2 (*a*) as a contour map. This contour map exhibits approximate odd symmetry with respect to the yaw angles, i.e. $\delta\eta(\beta_1,\beta_2) \approx \delta\eta(-\beta_1, -\beta_2)$, indicating that positive and negative yaw are equivalent for wake redirection purposes. Most of the power improvements are found in the first and third quadrants, where WT_1 and WT_2 are yawed towards the same direction. The peak power gains achieved in these two quadrants are 5.4% and 3.1%, corresponding to a yaw angle distribution of $[\beta_1, \beta_2] = [25^\circ, 15^\circ]$ (Case A) and $[\beta_1, \beta_2] = [-25^\circ, -20^\circ]$ (Case B), respectively. This decreasing trend of the optimal yaw angle distribution is consistent with the observations in Refs. [13,19].

Fig. 2 (*b*) shows the nondimensional power distributions in three representative cases. For the baseline non-yawed case, WT_2 and WT_3 suffer severely from the wake effects of WT_1, and the resultant power losses reach more than 60%. This value is even higher than that observed in large offshore wind farms (40–50%, e.g. Horns-Rev and Nysted) [23], largely because of the narrow turbine spacing ($5D$). In cases A and B, WT_1 sacrifices approximately 20% of its own power production to yaw, in exchange for steering the wake away from the downstream wind turbines. As a result, the wake-induced power losses experienced by WT_2 and WT_3 are reduced significantly, and the amount of power gained (30%–35% of P_0) overweights that sacrificed by WT_1, resulting in a net increase of the wind farm efficiency.

The hub-height velocity fields measured by PIV are shown in Fig. 3 for the aforementioned three cases. Wake-centre trajectories extracted by fitting the spanwise wake velocity profiles with a Gaussian function [24], are indicated as dash-dot black lines. In the non-yawed case, the middle-hub wake velocity contour exhibit a strict symmetry with respect to the $x-$ axis, and no wake deflection can be identified at $0 < x/D < 15$. This observation echoes with the odd symmetry shape of the power map shown in Fig. 2 (*a*). Therefore, the 2.3% difference in power production between cases A and B is most probably caused by the distinct wake shapes formed

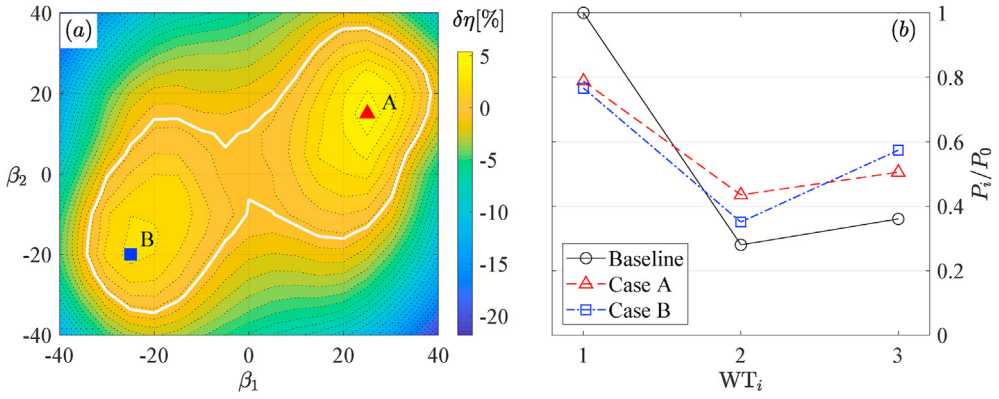

Fig. 2. (*a*) Relative power gain in the full-wake condition. The solid while line represents the contour line of $\delta\eta = 0$. Symbols 'A' and 'B' indicate the peak locations in the first and third quadrants, respectively. (*b*) Non-dimensional power distributions in three representative cases.

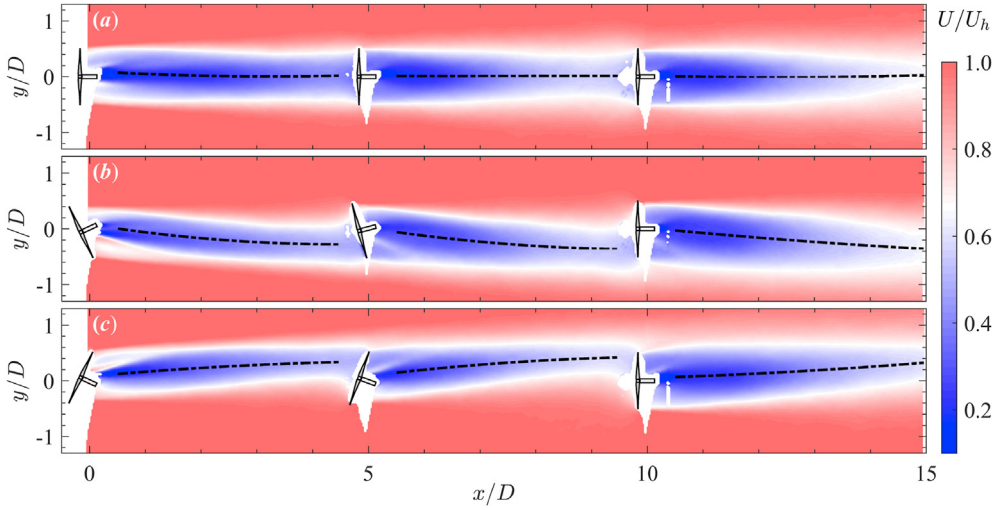

Fig. 3. Time-averaged wake velocity contours obtained from PIV measurements. (*a*) Baseline non-yawed case; (*b*) case A: $\beta_1 = 25^\circ, \beta_2 = 15^\circ$; (*c*) case B: $\beta_1 = -25^\circ, \beta_2 = -20^\circ$. The trajectories of wind turbine wakes extracted by fitting the spanwise velocity profile with a Gaussian function are superimposed as dash-dot black lines.

in positive and negative yaw [24,25], rather than the non-zero wake deflection at zero yaw angle postulated by Ref. [3] in a large-eddy simulation (LES) study of yawed wind turbine wakes. Alternatively speaking, if there does exist a non-trivial wake deflection in the non-yawed condition, the magnitude of the yaw angles in cases A and B would differ noticeably, and the contour line of $\delta\eta = 0$ in Fig. 2 (*a*) would be pinched from the middle since only one yawing direction is favourable for power improvement at the origin.

In Fig. 3 ($b - c$), WT_1 is yawed at a magnitude of 25°, and the resultant wake deflections at a downstream distance of $4.5D$ is $0.28D$. As a comparison, the wake deflection induced by WT_2 at a smaller yaw angle (i.e. 15-20°) reaches $0.4D$, even higher than that of WT_1. This phenomenon, termed as the 'secondary wake steering effect' by Ref. [26]; is most obvious for WT_3, which exhibits a significant wake deflection ($\approx 0.4D$ at $x = 15D$) even though the rotor disk is not yawed [19]. pointed out that without a proper implementation of this effect, the maximum power gain and the optimal yaw angle distribution predicted by the analytical model of AYC will be incorrect. Since the root of wake deflection lies in the transverse velocity, a viable way to reproduce the secondary wake steering is to incorporate the transverse velocity induced by upstream yawed wind turbines into the calculation of the wake trajectory of a downstream wind turbine. In other words, wake deflection superposition is required, analogous to the wake velocity deficit superposition [27,28].

Fig. 4 shows the spatial distributions of the turbulence intensity (I_u) measured at the hub height. For all the three cases, a high turbulence intensity is observed in the wake edges and shear layers, where the production rate of the turbulent kinetic energy (TKE) is much higher than the dissipation rate. The overall turbulence level in the wind farm accumulates in the streamwise direction, and an equilibrium state is reached after the third turbine row, which agrees well with the LES results reported by Ref. [29]. Since turbulent entrainment directly affects the wake recovery rate, it is not surprising that, in the baseline situation, the near-wake lengths ($\approx 2D$) of the downstream wind turbines are significantly shortened, with respect to the leading turbine

Compared to the non-yawed baseline case, the added turbulence levels in the yawed cases are relatively lower, as a result of the decreasing thrust coefficient [30]. Additionally, it is also noticed that, when the wind turbines are yawed or subjected to a partial wake condition (e.g. WT_3 in cases A and B), the turbulence intensity distribution across the wake becomes asymmetry. This will lead to uneven wake recovery rates in the two sides of the wake, and consequently an asymmetric wake velocity deficit profile in the spanwise direction. For future studies, the significance of this asymmetry in the power prediction of wind farms should be investigated, and if necessary, included in the analytical models of

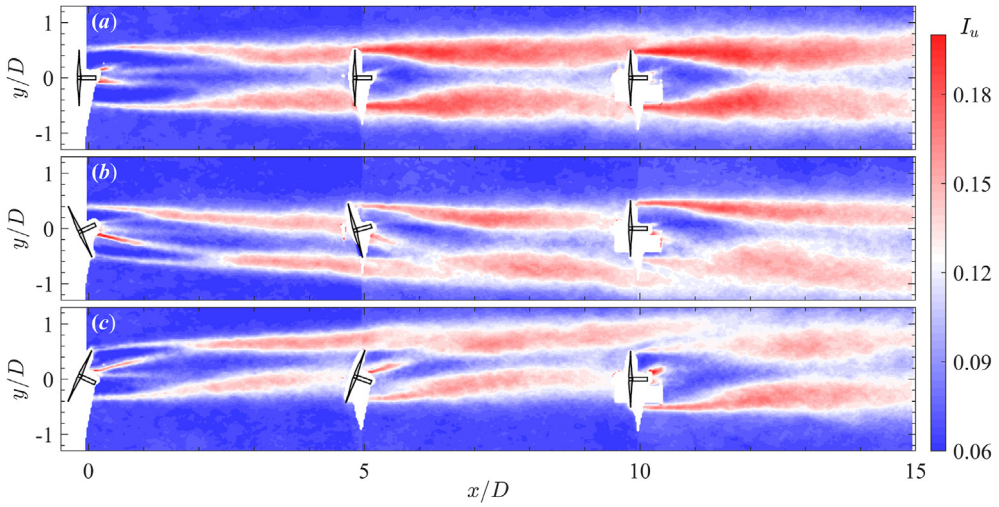

Fig. 4. Turbulence intensity distribution measured by PIV at the hub height. (*a*) Baseline non-yawed case; (*b*) case A: $\beta_1 = 25^\circ, \beta_2 = 15^\circ$; (*c*) case B: $\beta_1 = -25^\circ, \beta_2 = -20^\circ$.

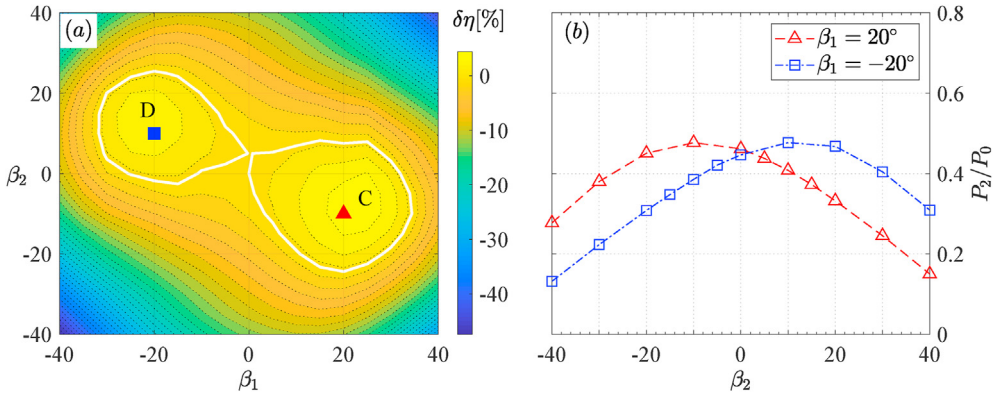

Fig. 5. (*a*) Relative variation of the total power production of WT_1 and WT_2 at different yaw angle combinations. The two symbols indicate the two peaks found in the second and fourth quadrants. The solid while line represents the contour line of $\delta\eta = 0$. (*b*) The non-dimensional power production of WT_2 at $\beta_1 = -20^\circ$ and 20°.

wind turbine wakes.

Before ending the present section, the authors would like to point out a minor flaw in the current yaw control strategy, i.e. the last wind turbine is maintained non-yawed to produce the 'maximum' power. Recall from the analysis of Fig. 3 that when the upstream wind turbines are yawed, a non-vanishing transverse velocity is induced in the wake. As a direct consequence of this transverse velocity, the local wind direction perceived by the downstream wind turbines are no longer along the *x*-axis, and thus, to capture the most wind power, the last wind turbine should also be yawed.

The above conjecture can be validated by only considering the first two wind turbines in the model wind farm. Fig. 5 (*a*) shows the relative variation of the total power of WT_1 and WT_2, at various yaw angle combinations. Contrary to the power map shown in Fig. 2 (*a*), positive power improvements are mainly found in the second and fourth quadrants. To achieve the maximum wind farm efficiency (peak 'C': $\delta\eta = 4\%$, peak 'D': $\delta\eta = 2.9\%$), WT_1 and WT_2 should be yawed in opposite directions. Without yawing the second wind turbine, the peak power production achieved by AYC would be 1% less. Fig. 5 (*b*) further shows the power production of WT_2 in cases of $\beta_1 = -20^\circ$ and 20°. Based on the centre shift of these two curves, it can be inferred that, due to the transverse velocity induced by the first wind turbine, the local wind direction perceived by the last wind turbine is altered by 10°. For wind farms with large row spacing, this value is expected to be smaller, since the transverse velocity decays with increasing downstream distance .

In the present investigation, WT_3 is kept non-yawed, mainly to keep the workload of seeking the optimal yaw angle list within an acceptable level. Otherwise, the number of variables will increase from two to three, and the experimental data points needed to construct a complete power map will be increased by approximately 10 times.

3.2. Partial wake condition

As mentioned earlier, six partial wake conditions are tested in the wind tunnel experiments, with $S_y = \pm D/3, \pm 2D/3$ and $\pm D$. After detailed examination, the authors found that the power maps and the wake velocity fields measured under these six conditions are morphologically similar. Thus, it becomes largely unnecessary to go over all of these cases and interpret the results tediously. Instead, in this section, the authors will only analyse the power map and the wake velocity fields in a representative case of $S_x = D/3$, and then focus on the influence of spanwise offset on the optimal yaw angle distribution and the maximum power production.

Fig. 6 (*a*) shows the relative variation of the wind farm efficiency at a spanwise offset of $S_y = D/3$. In contrast with the full-wake condition (Fig. 2 *a*), the power map obtained in the partial wake condition exhibits only one peak. Depending on the sign of the

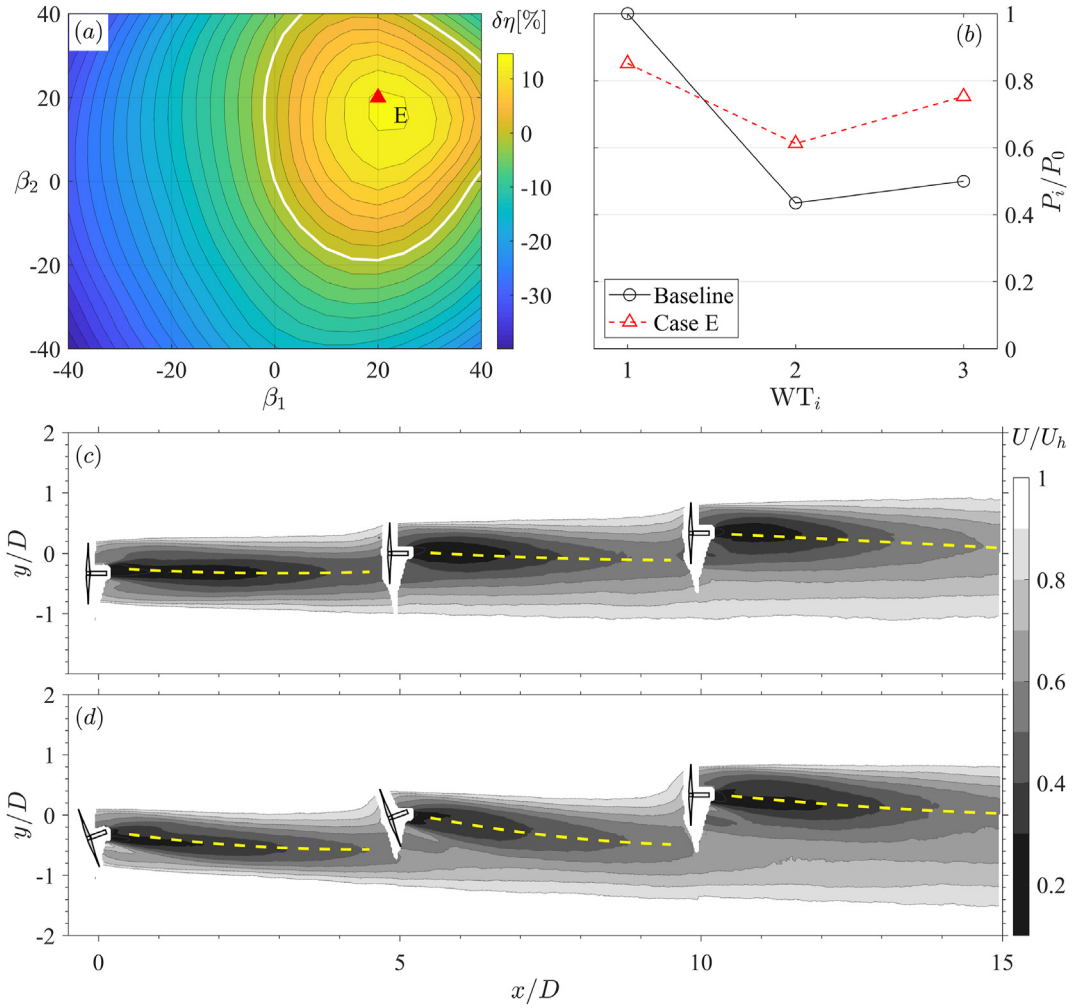

Fig. 6. Experimental results pertaining to a partial wake condition of $S_y = D/3$. (*a*) Contour map of the relative variation of the wind farm efficiency. The red triangle ('E') indicates the peak location. The solid white line is the contour line of $\delta\eta = 0$. (*b*) Power distributions in the baseline condition and Case E. (*c* – *d*) Time-averaged wake velocity contours in the baseline condition and Case E. The wake trajectories of wind turbines are indicated by the dash yellow lines.

spanwise offset (positive for the scenario sketched in Fig. 1 *a*), this peak is located either in the first quadrant or in the third, which is reasonable as only one yawing direction can redirect the wake away from the downstream wind turbines. The maximum power gain (14.6%) achieved at a spanwise offset of $S_y = D/3$ is much higher than that achieved in the full wake condition (5.4%), which agrees with the results reported by Refs. [4,10,31]. The optimal yaw angle combination (peak 'E') determined in a grid spacing of 5° is $\beta_1 = \beta_2 = 20^\circ$ (denoted as case E hereinafter). The power distributions for this optimal case and the baseline scenario are compared in Fig. 6 (*b*). As a result, in case E, the leading turbine produces 15% less power due to yaw, whereas each of the downstream turbines harvest 20% – 30% more power thanks to wake manipulation. In reference to the full wake condition, the gain to pain ratio seems to be boosted .

The mechanisms behind the performance change of AYC can be briefly interpreted by the wake velocity contours shown in Fig. 3 (*a*) and Fig. 6 (*c* – *d*). Specifically, without spanwise offsets, the downstream wind turbines are fully immersed in the wakes of their upstream wind turbines. Since the most power losses occur in the wake centre, deflecting the wakes sidewards by 0.3 – 0.4*D* does not dramatically increase the power productions of downstream wind turbines. As a comparison, in the baseline situation of $S_y = D/3$, the wake centres of the upstream wind turbines are already located near the rotor edges of the downstream wind turbines. Therefore, an additional wake deflection of 0.3 – 0.4*D* by AYC becomes sufficient to pull the downstream wind turbines out of the high power loss region (i.e. wake centre), leading to significant power improvements.

Additionally, it is noticed from Fig. 6 (*c*) that the wake centre of WT_3 gradually drifts towards the negative y – direction during the downstream propagation. This phenomenon has nothing to do the secondary wake steering effect detailed in section 3.1, as none of the upstream wind turbines are yawed. Rather, it is a consequence of the spanwise wind shear, which gives rise to an uneven wake recovery rate between the two sides of the wake.

Fig. 7 shows the absolute values of the optimal yaw angle distributions (denoted as $|\beta_{i,opt}|$) at different spanwise offsets. Note that these values are obtained by fitting the exact peak locations of the measured power maps with a two-dimensional Gaussian function, thus no longer limited to the discrete measurement grid values. For all the cases tested, the optimal yaw angle distribution shows a decreasing trend of $\beta_{1,opt} \geq \beta_{2,opt} \geq \beta_3 = 0$, consistent with the observations in Ref. [13]. As the spanwise offset ($|S_y|$) increases, $|\beta_{1,opt}|$ decreases monotonically, indicating the need for wake manipulation is reduced. $|\beta_{2,opt}|$ roughly follows the trend of

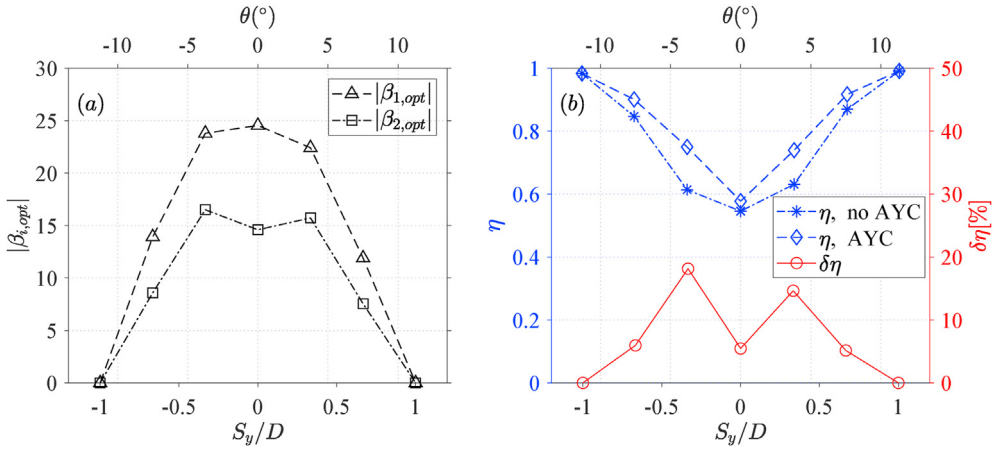

Fig. 7. (*a*) The optimal yaw angles ($\beta_{i,opt}$) at different spanwise offsets. Note that only the absolute values of the yaw angles are plotted, and the signs are positive (negative) in cases of $S_y \geq 0$ ($S_y < 0$). (*b*) Left axis: variation of the wind farm efficiency with spanwise offset. Right axis: the relative power improvement brought by AYC.

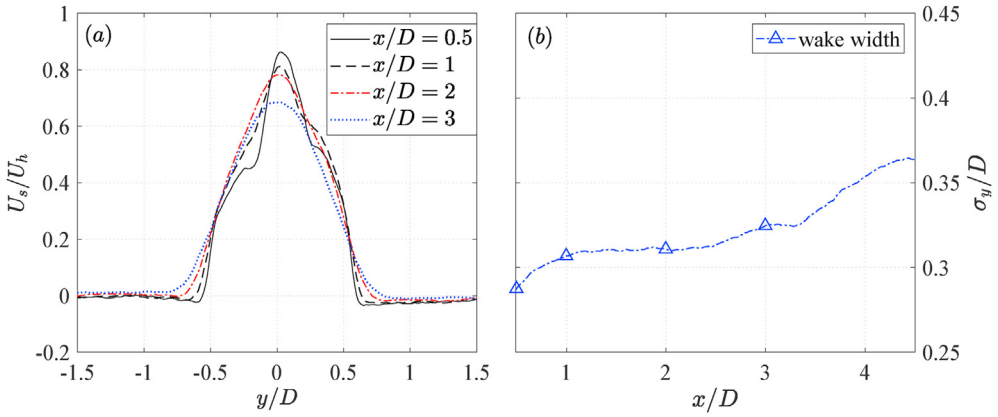

Fig. 8. (*a*) The near-wake velocity deficit profiles measured behind a stand-alone non-yawed wind turbine. (*b*) The streamwise variation of the spanwise wake width at $x/D < 4.5$.

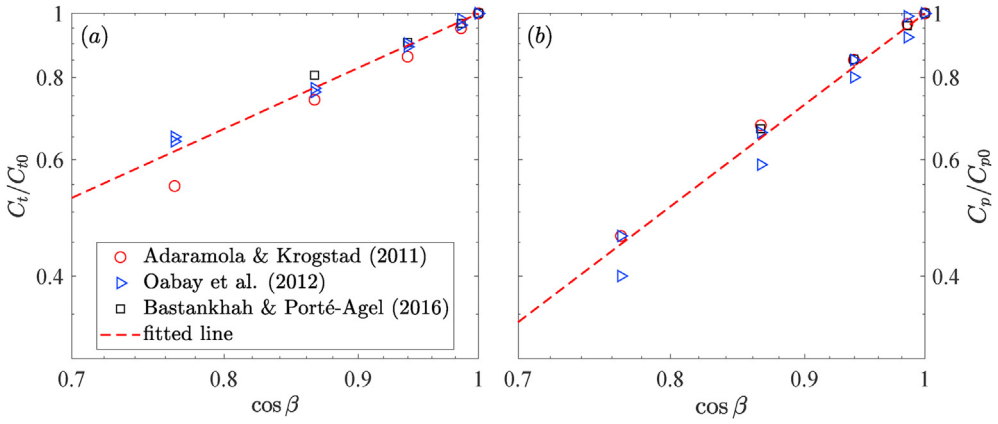

Fig. 9. Variation of (*a*) the power coefficient and (*b*) the thrust coefficient with yaw angle. The red dash lines indicate the linear fits: $C_t = C_{t0} \cdot (\cos\beta)^{1.8}$ and $C_p = C_{p0} \cdot (\cos\beta)^3$.

$|\beta_{1,opt}|$, whereas its peak value is reached at (see Fig. 8)$S_y = D/3$.

The wind farm efficiencies with and without implementation of AYC are plotted in Fig. 7 (*b*). These curves, as well as those shown in Fig. 7 (*a*) are approximately symmetric with respect to $S_y = 0$, which once again illustrates that there is no significant difference between the wake flow fields created at positive and negative yaw, at least from the power production perspective. As $|S_y|$ increases, the relative power improvement ($\delta\eta$) first rises and then drops. Particularly, at a spanwise offset of $|S_y| \geq 1$, the baseline wind farm efficiency is close to 1 and there is no room left for AYC to improve. The peak value of $\delta\eta$ (18%) is achieved at a moderate spanwise offset of $S_y = -D/3$, essentially, the situation where the maximum wake velocity deficits induced by the upstream wind turbines are located close to the rotor edges of the downstream wind turbines (refer to Fig. 6 *d*). If the wind turbine row direction is taken as the zero reference for all the cases, the data displayed in Fig. 7 can also be

plotted against the wind direction (denoted as θ): $\theta = \mathrm{atan}(S_y/S_x)$. As a result, the power losses caused by wake interactions mainly occur in the wind sector of 0±10°, and AYC is most effective at $\theta \approx \pm 4°$.

In [17]; a parametric wake model (FLORIS) is employed to optimize the power production of a three-row two-column wind farm (streamwise spacing: 7*D*). In contrast with our experimental observations, the highest yaw angle computed from their model occurs in the second wind turbine row, with a value as high as 40°. The discrepancy can be ascribed to the facts that the secondary wake steering effect is not accounted for by FLORIS [19], and the wake deflection expression used in their analytical model is the one proposed by Ref. [16]; which is known to overestimate the magnitudes of wake deflection [25,32]. Apart from these deficiencies, FLORIS manages to reproduce the decreasing trend of the optimal yaw angles with the increasing spanwise offset.

4. Analytical model development

A new analytical wind farm model for AYC is developed in this section, which reflects the recent progress in yawed wind turbine wakes and wake superposition principles. In reference to the previous analytical models for active yaw control [14,17], significant improvements are made in the following aspects:

1. A more accurate expression of the wake deflection is used, incorporating the influence of near-wake length and turbulence intensity.
2. The secondary wake steering effect on a downstream wind turbine is reproduced by superimposing the transverse velocities induced by all its upstream yawed wind turbines.
3. A novel momentum-conserved wake superposition principle is implemented to combine the wakes of individual wind turbines.

4.1. Wake expansion and deflection

The Gaussian wake model proposed by Ref. [33] is used to describe the streamwise evolution of individual turbine wakes. To enhance the model's performance in the near-wake region, the thrust coefficient in the original expression is multiplied by an error function to simulate the effect of streamwise pressure gradient [34], as follows

$$\frac{u_s^i}{u_0^i} = \left(1 - \sqrt{1 - \frac{C_t^i(1+\mathrm{erf}(x/D))}{16\sigma_y\sigma_z/D^2}}\right) \cdot \exp\left(-\frac{(y-y_c^i)^2}{2\sigma_y^2} - \frac{(z-z_h)^2}{2\sigma_z^2}\right) \tag{2}$$

where u_0^i is the mean wind speed experienced by WT_i at the hub height, and u_s^i is the wake velocity deficit; y_c^i represents the spanwise location of the wake centre (i.e. lateral wake deflection); σ_y and σ_z denote respectively the wake widths in the spanwise and vertical directions, which are typically modelled as quasi-linear functions of the streamwise coordinate [34]:

$$\begin{cases} \dfrac{\sigma_y}{D} = 0.35\cos\beta + k_w \ln\left[1 + \exp\left(\dfrac{x - x_{th}}{D}\right)\right] \\ \dfrac{\sigma_z}{D} = 0.35 + k_w \ln\left[1 + \exp\left(\dfrac{x - x_{th}}{D}\right)\right] \end{cases} \tag{3}$$

where, k_w, and x_{th} denote the wake growth rate and the near-wake length, respectively.

According to equation (3), the wake width is approximately constant in the near-wake and only starts to grow at $x > x_{th}$. This may sound odd to the readers, since, even in the near-wake region, the wake velocity deficits recovers as a result of turbulent entrainment. To resolve this concern, Fig. 8 shows the wake velocity deficit profiles measured behind WT_1 at zero yaw, as well as the streamwise variation of the spanwise wake width. Although the velocity profile changes non-trivially in the near-wake region, the majority of the wake velocity deficit is still confined in the spanwise range of $|y/D| \leq 0.5D$, resulting in a marginal growth of the wake width at $x/D < 3.5$. Therefore, it is safe to set the initial value in equation (3) as 0.35*D*, which approximately equals to the experimental wake width at $x = x_{th}$. For detailed expression of the near-wake length (x_{th}), please refer to Ref. [35]

The asymptotic wake spreading rate (k_w) is commonly written as a function of the turbulence intensity at the hub height (denoted as I_h) [2]:

$$\begin{cases} k_w = k_a \cdot I_h + k_b \\ I_h = \sqrt{I_0^2 + I_+^2} \end{cases} \tag{4}$$

where, k_a and k_b are two coefficients; I_+ denotes the added turbulence level brought by the upstream wind turbines, which is associated with the induction factor, ambient turbulence intensity and streamwise distance [30].

In [28]; only the influence of the nearest upstream wind turbine (say, WT*j*) is considered, and the following expression of the added turbulence intensity is used: $I_+ = 0.73 a_j^{0.83} I_0^{0.03} (l_x/D)^{-0.32} f(l_y)$, where l_x and l_y denotes respectively the streamwise and spanwise distance between WT_i and WT_j; $f(l_y)$ is an implicit top-hat function related to the overlapping area between the wake and the turbine. As a minor improvement to the original expression, $f(l_y)$ is directly written as a Gaussian function of the wake width in the present study, and an additional factor of u_0^j/U_∞ is added to account for the different reference wind speeds used by the wind turbines, as follows

$$I_+ = 0.73 a_j^{0.83} I_0^{0.03} \left(\frac{l_x}{D}\right)^{-0.32} \cdot \exp\left(-\frac{l_y^2}{2\sigma_y^2}\right) \cdot \frac{u_0^j}{U_\infty} \tag{5}$$

By performing a linear regression on the wake spreading rates obtained from LES, the two coefficients in equation (4) are determined as $k_a = 0.38$ and $k_b = 0.004$ in Ref. [28]. Nevertheless, according to the field measurement data in Ref. [36]; the best fit for equation (4) is $k_a = 0.35$ and $k_b = 0.0$. The discrepancy in these values, seemingly small, can significantly affect the results of the present analytical model. Ideally, *a priori* calibration of the two parameters against some known values of k_w (e.g, those fitted from PIV measurements) should be carried out, to minimize the power prediction error. However, the experimental data available in this study are ineligible for such purpose, because of the interference of downstream wind turbines and the long near-wake length ($\approx 4D$). As an alternative, *a posteriori* tuning of the two parameters against the power measurement data presented in section 3 are executed, and the final values adopted by the present analytical model are $k_a = 0.35$ and $k_b = 0.004$, respectively.

With the efforts made above, the only unknown remaining in equation (2) is the lateral wake deflection (y_c^i), which can be integrated from the slope of the wake trajectory, as follows

$$y_c^i = \int \frac{\mathrm{d}y_c^i}{\mathrm{d}x}\mathrm{d}x = \int \frac{V_c^i(x)}{u_0^i}\mathrm{d}x \tag{6}$$

where, the secondary wake steering effect is accounted by defining V_c^i as the total transverse velocity induced at the wake centre of WT_i, by not only itself but also all its upstream partners. Note, in practice, the pivoting point of wind turbines in yaw motion is not exactly located at the centre of the rotor disk, and a small lateral shift of the rotor disk centre will occur inevitably due to yaw. This physical shift, which is non-trivial for the WIRE-01 turbine (0.1D at $\beta = 30^\circ$), should be set as the initial value for wake deflection integration.

According to the wake deflection superposition method developed by Ref. [37]; the total transverse velocity is a weighted sum of the individually induced transverse velocity (denoted as ν^j):

$$V_c^i(x) = \sum_j \frac{u_0^j}{u_0^i}\nu^j\left(x, y_c^i\right) \tag{7}$$

where, j loops through all the wind turbines involved.

Currently, four analytical models are available to compute the transverse velocity induced by a stand-alone yawed wind turbine [16,25,32,34]. Except for the one proposed by Ref. [16] which has been demonstrated to overestimate the experimental values of wake deflection [32], all the other three models can reasonably reproduce the wake trajectories of yawed wind turbines with a typical error of less than 0.1D, thus equivalent in performance. For the sake of simplicity, the following expression adapted from Ref. [34] is used:

$$\nu^j(x,y) = \frac{-C_t^j u_0^j \sin\beta}{8\sigma_y\sigma_z/\sigma_{y0}\sigma_{z0}} \cdot \left[1 + \mathrm{erf}\left(\frac{x}{D}\right)\right] \cdot \exp\left(-\frac{\left(y - y_c^j\right)^2}{2\sigma_y^2}\right) \tag{8}$$

where, σ_{y0} and σ_{z0} represent the initial wake width in the spanwise and the wall-normal directions, respectively. Compared to the original expression, two modifications are made. One is the drop-out of $\cos(\beta)^2$ term due to the different definitions of C_t. The other is the addition of a Gaussian function, which is intended to spread the transverse velocity in the spanwise direction and thus extend the applicability of the model to partial wake conditions.

Additionally, it should be noted that, although the experimental results in section 3.1 have demonstrated that the transverse velocity induced by an upstream yawed wind turbine will slightly alter the local wind direction perceived by the downstream wind turbines, this effect is deemed small and thus not accounted for in the present model.

4.2. Wake superposition and power production

To compute the total wake velocity deficit (U_c), the momentum-conserving wake superposition method proposed by Ref. [37] is invoked,

$$U_s(x,y,z) = \sum_i \frac{u_c^i(x)}{U_c(x)} u_s^i(x,y,z) \tag{9}$$

where, u_c^i and U_c denote respectively the characteristic convection velocity of the individual and the combined wakes, given by

$$\begin{cases} u_c^i(x) = \dfrac{\iint (u_0^i - u_s^i)u_s^i \mathrm{d}y\mathrm{d}z}{\iint u_s^i \mathrm{d}y\mathrm{d}z} \\ U_c(x) = \dfrac{\iint (U_h - U_s)U_s \mathrm{d}y\mathrm{d}z}{\iint U_s \mathrm{d}y\mathrm{d}z} \end{cases} \tag{10}$$

Equation (9) and equation (7) share a similar form. Both state that during the combination of individual wakes, the one associated with a higher hub velocity shall be represented by a larger weight, which is reasonable because the streamwise momentum deficit (spanwise momentum) carried by an individual wake is proportional not only to the wake velocity deficit (transverse velocity) but also to the mean wake convection velocity [38]. Additionally, it should be noticed that the convection velocity for the combined wake (U_c) remains unknown prior to the wake superposition stage, and thus several iterations are needed to solve the total wake velocity deficit out of equations (9) and (10) (refer to Ref. [37] for more information).

Based on the total wake velocity deficit, the non-dimensional available power at the location of each wind turbine (x_t^i, y_t^i) can be computed [24],

$$\begin{aligned} f_{AP}^i &= \iint_G (U_h - U_s)^3 \mathrm{d}y\mathrm{d}z \Big/ \iint_G U_h^3 \mathrm{d}y\mathrm{d}z \\ G &: \left(y - y_t^i\right)^2 + (z - z_h)^2 \le D^2/4 \end{aligned} \tag{11}$$

For yawed wind turbines, it is a common practice to write the thrust and power coefficients as cosine functions of the yaw angle [10,12], resulting in the following two equations:

$$\begin{cases} C_t^i = C_{t0} \cdot (\cos\beta_i)^p \\ C_p^i = C_{p0} \cdot (\cos\beta_i)^q \end{cases} \tag{12}$$

where, C_{t0} and C_{p0} denote the thrust and power coefficients at zero yaw (0.82 and 0.31 for the WIRE-01 turbine used in study); p and q are the cosine exponents related to the decay rates of the thrust and power coefficients at increasing yaw.

In Fig. 9, the experimental values of C_t/C_{t0} and C_p/C_{p0} reported by Refs. [11,12,25] are plotted against $\cos(\beta)$ in the logarithmic scale. Note that all these data points are extracted at the optimal tip speed ratios of the wind turbines. As a result, an approximate linear relationship is exhibited between the normalized coefficients and the cosine value of the yaw angle in the range of $0 \le \beta \le 40^\circ$. By performing a linear regression on these datasets, the values of p and q are determined to be 1.8 and 3, respectively. These two values, which will be used throughout this study, are under no means universal. The control scheme (variable-speed or dual-speed) and the blade geometry, particularly the lift-drag characteristics of the airfoil used in design, should be accounted during the selection of these two values. For variable-speed wind turbines designed with an airfoil exhibiting a high lift-to-drag ratio in a wide range of angle of attack (AOA), their power coefficients are likely to remain high in yawed conditions, thus resulting in a small q value. However, for dual-speed wind turbines that are optimized at a specific operating point of the airfoil, a high value of q is expected .

Additionally, it should be noted that in the present analytical model, the incoming wind profile is assumed to be homogenous, and the time-averaged wind speed at the hub height (U_h) is taken as the reference velocity to compute the wake velocity deficit. In order to incorporate the influence of vertical wind shear in field, two modifications can be made. First, in equation (11), while

computing the available power, the hub-height wind speed (U_h, constant) can be replaced by the spatially-dependent wind profile (denoted as U_{in}, as a function of the vertical coordinate z). Second, the expression of the turbine power coefficient, i.e. equation (12), should be corrected to reflect the adverse effects induced by wind shear. Specifically, with wind shear, the local wind speed perceived by the blades varies with azimuthal angle, leading to a periodical variation of the tip speed ratio in one cycle. Since the peak power coefficient can only be reached at a particular tip speed ratio, the time-averaged power production in the case of non -uniform wind condition is expected to be lower than that in uniform inflow.

4.3. Power optimization and model validation

With the efforts made in the previous two sub-sections, we are able to predict the power production of a wind farm at any yaw angle distribution. To optimize the total power production, a gradient ascent algorithm is used in this study. Although this algorithm tends to be stuck in the local peak, the authors expect that, by specifying an *appropriate* yaw angle distribution as the initial condition, the local peak found by the algorithm will be close to the global peak. For regular-layout wind farms in rhomboid or rectangular shapes, such a favourable yaw angle distribution is given by the following equation,

$$\beta_i = \pm\beta_{max}\frac{i}{N} \tag{13}$$

where β_{max} is the maximum yaw angle value interpolated from Fig. 7 (a), as a function of the wind direction; i is the index of the wind turbine, numbered from upstream to downstream. The sign of yaw angle should be selected in such a way that the resultant wake deflection adds up to the existing spanwise offset. During the search of the optimal yaw angle distribution, the initial step size is set as 5°, and this step size is reduced by a factor of 2 each time the total power computed in the current step is lower than the previous step (i.e. scenario of running over the peak). The search is terminated when the step size drops below 0.1°.

Fig. 10 (a) shows the full-wake power maps obtained from the experiments and the analytical wind farm model. Since these maps are approximately odd functions of the yaw angle distribution, only the right half is compared. Overall, the model prediction results agree quite well with the experimental data, with the positive power improvement region correctly reproduced and the optimal yaw angle combination successfully captured. The maximum power improvement predicted by the analytical model is 6.9%, slightly higher than the experimental value (5.4%). Fig. 10 (b) further compares the relative power improvement at different spanwise offsets. As illustrated, all the experimental data collapse on the smooth dual-peak curve computed by the analytical model, resulting in a mean prediction error of less than 2% .

5. Parametric studies of AYC

The parameters influencing the effectiveness of AYC include but are not limited to the wind direction (spanwise offset), number of rows/columns, streamwise spacing, and turbulence intensity. Except for the wind direction which has been investigated experimentally in section 3, the effects of other parameters on AYC still remain unknown and thus will be explored sequentially in the following section using the proposed analytical model.

5.1. Number of rows

A single-column wind farm working in full-wake condition is considered. The turbulence intensity (7.2%), the streamwise spacing ($5D$) and the thrust coefficient under non-yawed conditions (0.82) are kept the same as those in the experiments, leaving the row number (denoted as N_x) as the only independent variable. The left row of Fig. 11 shows the optimal yaw angle distributions predicted by the analytical model at $N_x = 5$, 10 and 15. In all these cases, the optimal yaw angle distributions show similar trends. Specifically, the leading and the last wind turbines are yawed at approximately 30° and 0°, respectively. For the turbines in between, their yaw angles are maintained at about 20 decrease, decreasing slightly while moving downstream. These observations are consistent with the experimental data reported in section 3 and [13].

The power distributions in the baseline and optimal cases are compared in the right row of Fig. 11. Without yaw, the second wind turbine produces the least power, as a result of the high wake velocity deficit and the low wake recovery rate behind WT_1. Further downstream, the wake growth rate increases gradually because of the added turbulence intensity, and an equilibrium state of power production is reached at turbine row numbers larger than 3. In reference to the baseline case, the power distribution curves in the optimal cases seem to be lifted by 0.1 as a whole, excluding the first wind turbine whose power production is reduced due to yaw. For the present settings of the turbulence intensity and streamwise spacing, the equilibrium values of P_i/P_0 for the baseline and optimal cases are 0.38 and 0.47, respectively.

Fig. 12 (a) shows the optimal yaw angle of the leading turbine ($\beta_{1,opt}$) and the relative power improvement in the range of $2 \le N_x \le 15$. As the row number increases, both $\beta_{1,opt}$ and $\delta\eta$ increase asymptotically. The limit value for the leading-turbine yaw

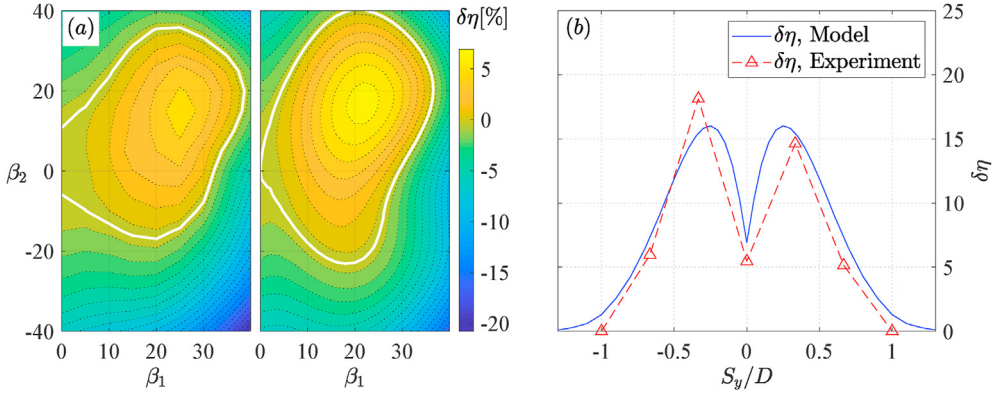

Fig. 10. (a) Comparison of the full-wake power maps obtained from the experiments (left half) and the analytical model (right half). The solid white lines are contour lines of $\delta\eta = 0$. (b) Model predictions of the relative power improvement at different spanwise offsets.

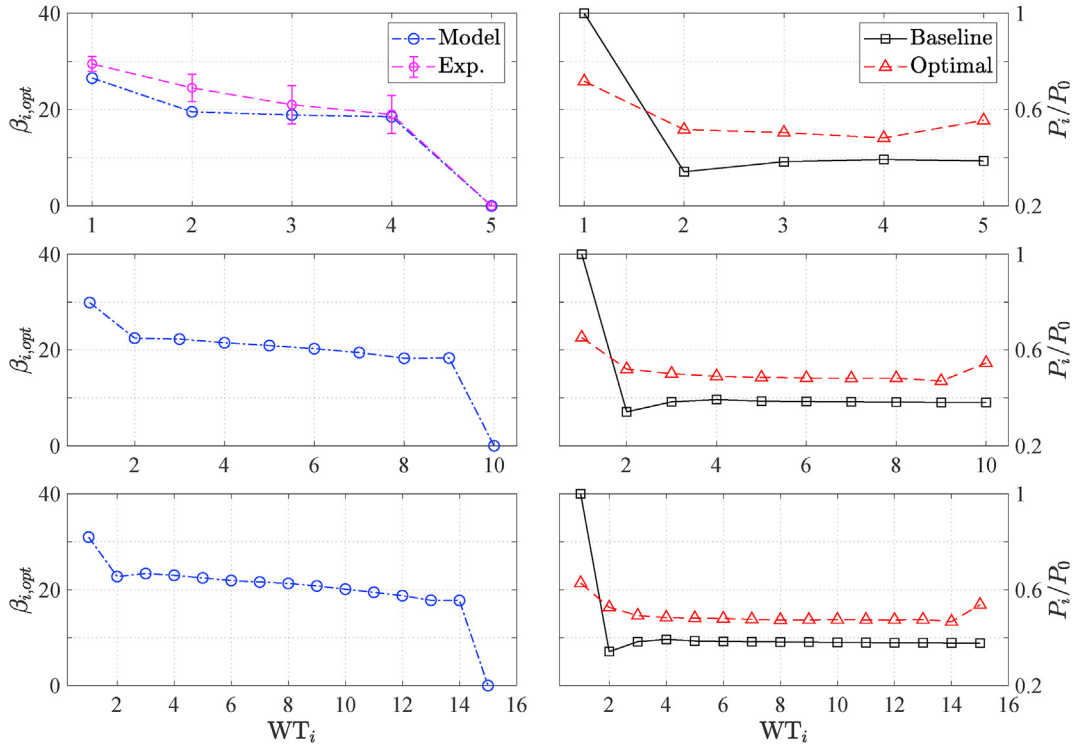

Fig. 11. Left column: from top to bottom, optimal yaw angle distributions at $N_x = 5$, 10, and 15 respectively. Right column: from top to bottom, comparison of the power distributions between the baseline non-yawed case and the optimal case at $N_x = 5$, 10, and 15 respectively. The experimental data plotted in the top-left corner are extracted digitally from Ref. [13].

angle is approximately 32° and can be explained theoretically from the relation between yaw angle and wake deflection. Specifically, substituting equation (12) into equations (8) and (7), the magnitude of wake deflection for a stand-alone wind turbine can be written as a function of the yaw angle,

$$y_c = \Phi \cdot C_{t0} \cos(\beta)^p \sin(\beta) \tag{14}$$

where Φ denotes the remaining terms (wake width, error function, etc) dependent mainly on the streamwise coordinate. By treating Φ as a constant and equating the derivative of equation (14) to zero, the critical yaw angle which gives the maximum wake deflection (β_{cr}) can be solved:

$$\beta_{cr} = \text{atan}(1 / \sqrt{p}) \tag{15}$$

The meaning of this critical yaw angle is obvious: in the practical implementation of AYC, under no circumstance, should the yaw angle of any wind turbine exceed the critical value. Once this critical value is exceeded, the wind turbine not only loses more power, but also induces less wake deflection. For a typical value of $p = 1.8$, β_{cr} is estimated to be 29°. This value is lower than the value shown in Fig. 12 ($\approx 32°$), largely because Φ is assumed to be a constant during the derivation of equation (15). Strictly speaking, this assumption does not hold. Except for the trigonometric term (i.e. $\cos(\beta)^p \sin(\beta)$), the spanwise wake width hidden in the term Φ (see equation (3)) is also associated with the yaw angle, albeit weakly.

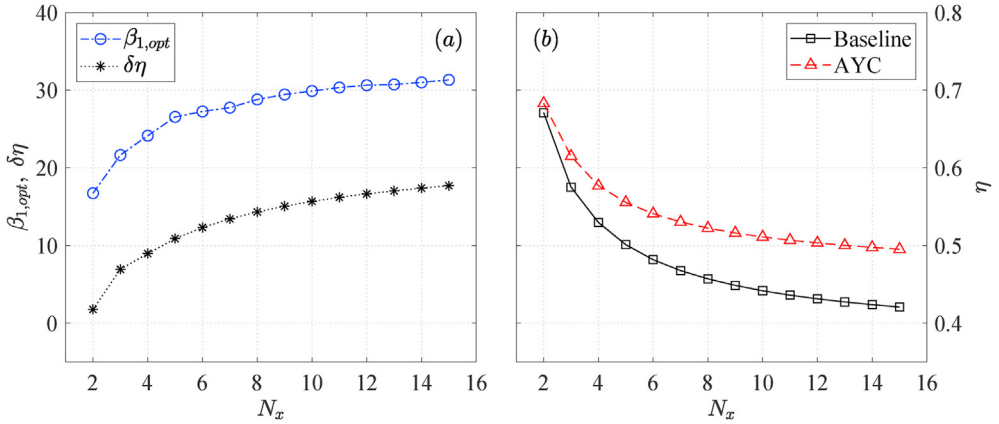

Fig. 12. (*a*) Variation of the leading-turbine yaw angle and the relative power improvement with the number of turbine rows. (*b*) Comparison of the wind farm efficiency with and without implementation of active yaw control.

The asymptotic growth of the relative power improvement at increasing number of rows can be best interpreted from Fig. 12 (*b*), where the wind farm efficiencies with and without AYC are plotted. In both cases, a monotonic decrease of the wind farm efficiency is observed, with the lower limit set by the equilibrium values of P_i/P_0 shown in Fig. 11. Based on the relative difference between the two equilibrium values (0.38 and 0.47), the upper limit of $\delta\eta$ at infinite number of rows is inferred to be 24%. For small values of N_x, the relative power improvement is less, due to the high baseline wind farm efficiency. Particularly, at $N_x = 5$, the present model predicts a relative power improvement of 11%, which is lower than the experimental value (17%) reported by Ref. [13]; as a result of the different turbulent intensities used in this and their studies (rounded to two-digit accuracy: 7.2% vs. 6.5%).

5.2. Number of columns

The main difference between AYC in single-column and multiple-column wind farms is that in the latter case, as the upstream wind turbines yawed, their wakes have a possibility to hit the wind turbines in nearby columns, which will counteract part of the benefits earned by wake steering. To investigate how significant this effect is to active yaw control, a five-row wind farm, where the wind turbines are spaced uniformly in the streamwise and spanwise directions at 5*D* distance, is considered. Fig. 13 shows the variations of the baseline wind farm efficiency and the relative power improvement in the wind sector of $0^\circ \le \theta \le 15^\circ$, for three different column numbers (N_y=1, 3, 5). As a result, the effect of increasing column number can only be felt at $\theta > 10^\circ$, when the wake created by the first wind turbine in a column starts to intersect the last wind turbines in the adjacent columns (i.e. $\theta \approx \mathrm{atan}(1/N_x)$). This column-to-column wake interaction leads to a noticeable decrease in the baseline wind farm efficiency by up to 10% at $\theta = 15^\circ$. In contrast, the influence of column interaction on the relative power improvement achieved by AYC is negligible, which can be ascribed to the fact that when column-to-column wake interaction occurs (i.e. $\theta > 10^\circ$), the wakes of upstream wind turbines are no longer interfering or at least weakly interfering the wind turbines in the subsequent row. In such a situation, there is little room for AYC to improve, regardless of the number of columns .

Additionally, the authors want to stress that the magnitude of wake deflection in the far downstream is a bounded value determined by the rotor diameter, yaw angle, thrust coefficient and wake growth rate. This value can be integrated from equation (8), as follows

$$y_{c,\infty} \approx \int_0^{+\infty} \frac{C_t \sin\beta \cdot \sigma_{z0}^2}{4(\sigma_{z0} + k_w x)^2} \mathrm{d}x \approx \frac{C_{t0}\sigma_{z0}\sin\beta(\cos\beta)^p}{4k_w} \tag{16}$$

where, the error function is discarded during the derivation, and the wake widths in both the spanwise and vertical directions are simplified as a linear function of the streamwise coordinate, i.e. $\sigma_{z0} + k_w x$. Plugging the typical values of the parameters used in this study into equation (16), the asymptotic wake deflection at $\beta = 30^\circ$ is estimated to be 0.8*D*. This value is far less than the typical column spacing of $5 - 7D$ in large wind farms, which, further justifies our previous conclusion that column-to-column wake interactions have negligible influence on the effectiveness of AYC .

5.3. Turbulence intensity

A five-row single-column wind farm (streamwise spacing: 5*D*) is used as a test bench to examine the effect of turbulence intensity on active yaw control. The wind farm efficiency and the relative power improvement are plotted in Fig. 14 for three representative turbulence levels (low: 5%, medium: 7.2%, and high: 10%). As expected, in the baseline condition, a high turbulence level is beneficial to the improvement of wind farm efficiency, due to the high wake recovery rate. However, this benefit is limited to the wind sector of $0 - 6$ degrees, beyond which the power production starts to decrease slightly with increasing turbulence level. To reveal the mechanism behind this inversion, the velocity deficit experienced by the second wind turbine in partial wake conditions is analysed, which, according to equation (2), can be written as follows

$$\frac{U_s}{U_h} \approx \left(1 - \sqrt{1 - \frac{C_{t0}D^2}{16\sigma_y^2}}\right) \cdot \exp\left(-\frac{(S_x\theta)^2}{2\sigma_y^2}\right) \tag{17}$$

where the spanwise distance between WT_1 and WT_2 (i.e. $S_x\tan\theta$) is approximated by $S_x\theta$. Evidently, the impact of turbulence intensity (wake growth rate) on power production is introduced by the wake width. With increasing turbulence intensity, the wake width also increases, whereas the wake velocity deficit does not necessarily decrease, since equation (17) is only a monotonic function of the wake width in full-wake conditions ($\theta = 0^\circ$). For partial wake situations where $\theta \neq 0^\circ$, the first and the second terms in the right side of equation (17) vary oppositely, i.e. one decreasing and the other increasing with the wake width. The final trend of the wake velocity deficit depends on the competition of these two terms. At

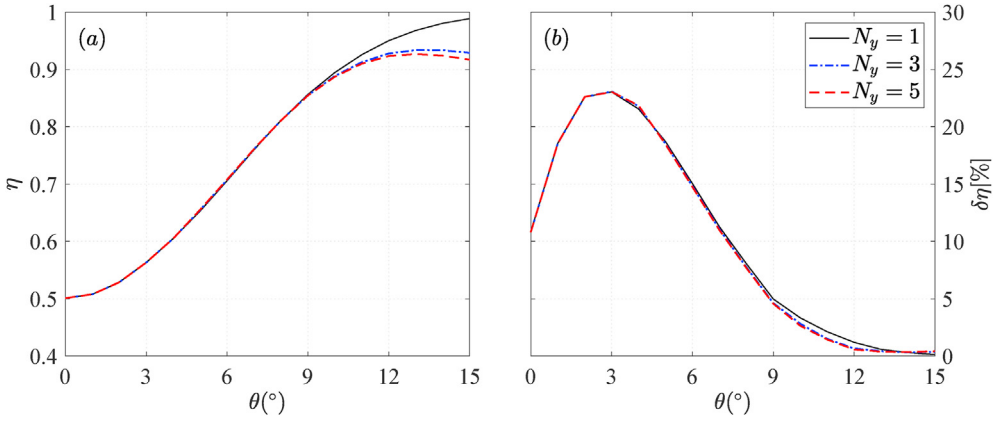

Fig. 13. Variations of (*a*) the baseline wind farm efficiency and (*b*) the relative power improvement in the wind sector of $0^\circ \le \theta \le 15^\circ$, for three different column numbers.

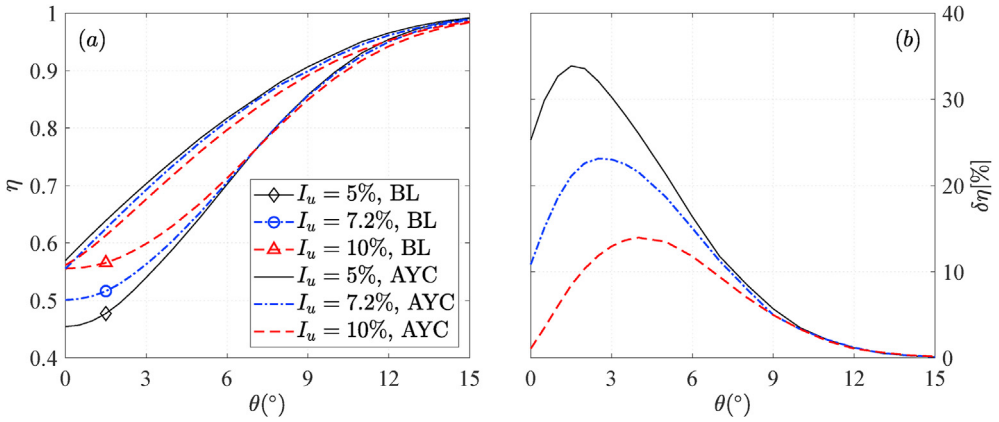

Fig. 14. Variations of (*a*) the wind farm efficiency and (*b*) the relative power improvement in the wind sector of $0^\circ \le \theta \le 15^\circ$, at three representative turbulence levels.

large values of θ, the exponential term dominates, leading to a slightly increasing trend of the wake velocity deficit and thus a decreasing power production, as illustrated by Fig. 14 (*a*).

When active yaw control is applied, the wind farm efficiency at the three turbulence levels are boosted approximately to the same values, and the relative power improvement is inversely proportional to the turbulence intensity, indicating that AYC is more effective in low-turbulence environments. Actually, this is largely expected from equation (14), where the asymptotic wake deflection in the far downstream is demonstrated to decrease with the increasing wake growth rate.

Additionally, it is noticed that the peak location of $\delta\eta$ shifts from $\theta = 1.5^\circ$ to $\theta = 4^\circ$, when I_u increases from 5% to 10%. This shift can be explained by considering a two-turbine wind farm operating in different wind direction. When AYC is applied to this wind farm, WT_1 loses its power production to yaw, in exchange for a certain amount of wake deflection. Now, let us take a unit wake deflection, and investigate in which wind direction the second turbine would gain the most power. Mathematically, this is a sensitivity problem, and the answer depends on the spanwise velocity gradient at the hub level of WT_2. Going back to equation (17) and taking the derivative of U_s with respect to $|\theta|$, the following equation can be derived,

$$\frac{\mathrm{d}U_s}{\mathrm{d}(|\theta|)} \approx \Psi \cdot |\theta| \exp\left(-\frac{\theta^2}{2\sigma_y^2/S_x^2}\right) \tag{18}$$

where Ψ denotes the remaining terms that are independent of θ. Equation (18) has three extremes, one minimum at $\theta = 0^\circ$ and two maxima at $\theta = \pm\sqrt{2}\sigma_y/S_x$. The minimum point explains the low effectiveness of AYC in full-wake conditions, whereas the two maxima corresponds to the partial wake conditions where the peak power improvement is reached (see Fig. 7 *b*). These partial wake conditions have a spanwise offset of $S_y = \pm\sqrt{2}\sigma_y$. In connection with Fig. 14 (*b*), we can conclude that the peak location shift is mainly due to the increasing wake width at the high turbulence level.

5.4. Streamwise spacing

The effects of streamwise spacing are treated in a similar fashion as that of turbulence intensity. Three typical values of S_x (i.e. 5*D*, 7*D*, and 9*D*) are studied, and the corresponding active yaw control results are compared in Fig. 15. With increasing streamwise spacing, the baseline wind farm efficiency is improved in a wide range of wind sector ($0^\circ \le \theta \le 15^\circ$), unlike the increase of turbulence intensity, whose benefits are limited to the wind sector of 0 – 6 degrees (Fig. 14 *a*). This difference, once again, originates from the exponential term in the right side of equation (17), $\exp(-(S_x\theta)^2/2\sigma_y^2)$. As can be easily demonstrated, when the wake growth rate/turbulence intensity is fixed, this exponential term varies marginally with the streamwise spacing, leaving equation (17) as a monotonic function of S_x, irrespective of the value of θ

Since the streamwise spacing modifies the strength of wake interactions in the baseline condition, it is not surprising to notice from Fig. 15 (*b*) that, as the streamwise spacing increases, the relative power improvement decreases. Particularly, in the case of $S_x = 9D$ and $\theta = 0^\circ$, active yaw control completely loses its effectiveness. Moreover, we notice that the peak locations of $\delta\eta$ seem to be insensitive to the variations of streamwise spacing, at least in the range of $5D < S_x < 9D$. Referring to the theoretical analysis made in the previous section, the maximum power gain in AYC is attained at a wind direction of $\theta = \sqrt{2}\sigma_y/S_x$. Since the wake width σ_y is a quasilinear function of the streamwise distance S_x, the peak location determined by the ratio of these two parameters is roughly a constant, dependent only on the wake growth rate/turbulence intensity .

6. Application to Horns-Rev wind farm

In the previous section, we have investigated how various parameter could affect the effectiveness of active yaw control. In this section, the proposed analytical model is further applied to the Horns-Rev wind farm [23]. As sketched in Fig. 16, this offshore wind farm has a rhomboid layout, consisting of 80 wind turbines arranged in 10 rows (R1, R2, R3…) and 8 columns (C1, C2, C3…). The turbine spacing is 7*D* along both row and column directions. For the purpose of baseline efficiency validation, major parameters pertinent to power production are inherited from the LES study of [29]. Specifically, the wind speed and the ambient turbulence level are kept as 8 m/s and 7.7%, respectively. The thrust coefficient of the wind turbine at zero yaw is fixed to 0.8, and the streamwise distance between the turbine tower and the rotor disk centre is assumed to be 0.1*D*. Other parameters, e.g. *p*, *q*, k_a and k_b, remain the same as in section 4 .

Fig. 17 (*a*) shows the wind farm efficiencies at different wind directions. In the baseline situation, significant power losses up to 30%–40% are observed in the four wind directions indicated in Fig. 16 ($\theta = 173^\circ, 222^\circ, 270^\circ, 312^\circ$), where full-wake interactions occur within a streamwise distance of 10*D*. The baseline efficiency

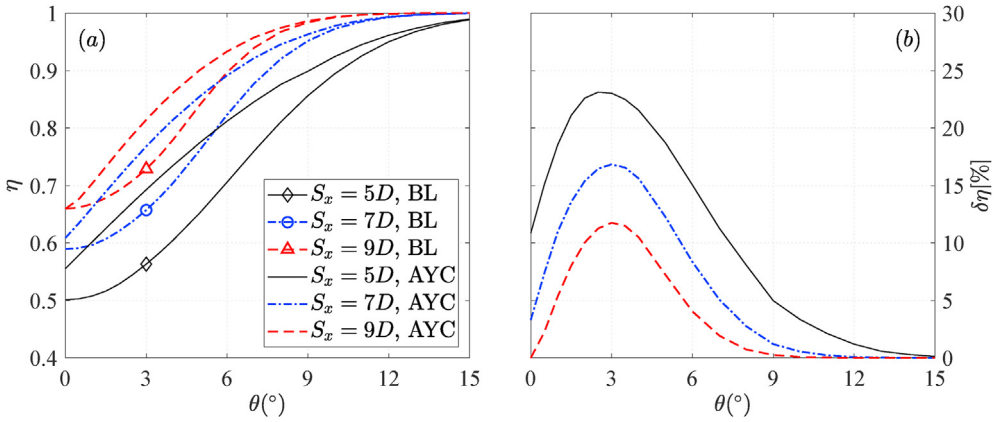

Fig. 15. Effects of streamwise spacing on (*a*) the wind farm efficiency and (*b*) the relative power improvement in the wind sector of $0^\circ \leq \theta \leq 15^\circ$.

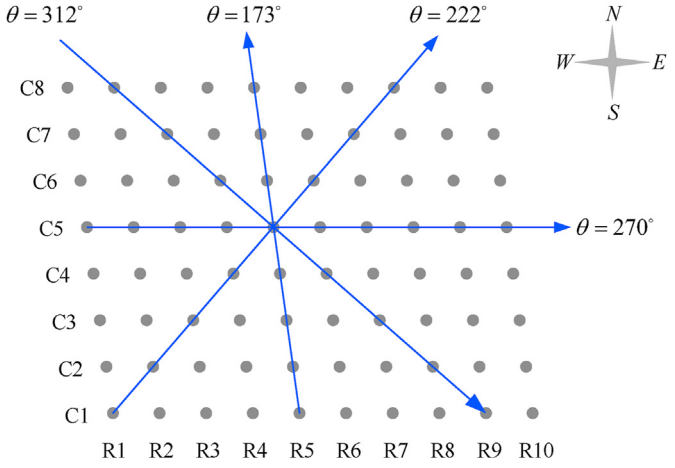

Fig. 16. Sketch of Horns-Rev wind farm. Wind turbines are represented by dark circles. Solid lines indicate the wind directions involving full-wake interactions within a streamwise distance of 10*D*.

obtained from the analytical wind farm model agrees well with that predicted by LES [29], and the mean error between these two datasets is less than 3%. When active yaw control is deployed, the power production of the wind farm is improved noticeably. Nevertheless, this power improvement is confined in the vicinity of the four wind directions mentioned earlier on. For other wind directions, the wake interactions are rather weak, and the relative power improvement achieved by AYC can be neglected (< 1%, see Fig. 17 *b*). Comparing the values of $\delta\eta$ for different wind sectors, we can see that the conclusions drawn in section 4 still hold. Namely, the maximum power improvement always occurs in the partial wake conditions (e.g., $222^\circ \pm 3^\circ$, $270^\circ \pm 4^\circ$), and the peak value of $\delta\eta$ is inversely proportional to the streamwise distance between two interacting wind turbines.

The relative variation of the annual power production can be computed as follows,

$$\Delta\eta = \frac{\int_0^{2\pi} g(\theta)(\eta_A - \eta_B)\mathrm{d}\theta}{\int_0^{2\pi} g(\theta)\eta_B \mathrm{d}\theta} \tag{19}$$

where $g(\theta)$ denote the probability density function of the wind direction; η_A and η_B are the wind farm efficiencies with and without active yaw control. Considering a simple case where the turbulence intensity is always 7.7% and the wind direction is distributed uniformly in a year, the annual power improvement brought by active yaw control is estimated to be 1.8%. In practice, this value is highly unlikely to be reached, as wind farms are usually designed in such a way that the power losses associated with the dominant wind directions are minimised. Nevertheless, it gives us an idea of what we can expect from active yaw control.

The optimal yaw angle of the leading wind turbine in the wind farm ($\beta_{1,opt}$) is shown in Fig. 17 (*c*) for cases with noticeable power improvement (criterion: $\delta\eta \geq 1\%$). Consistent with the theoretical analysis performed in section 5.1, the maximum value of $\beta_{1,opt}$ is always below 30°, i.e. the threshold value dictated by equation (15). As the wind direction departs from the directions involving full-wake interactions (e.g, $173^\circ \rightarrow 181^\circ$, $270^\circ \rightarrow 280^\circ$), the optimal yaw angle of the leading wind turbine exhibits an approximately decreasing trend, which agrees well with the experimental results shown in Fig. 7. Comparing the peak values of $\beta_{1,opt}$ in different wind sectors, it seems that the streamwise spacing between two interacting wind turbines has no explicit influence on the magnitude of the optimal yaw angle.

Fig. 18 shows the optimal yaw angle and power distributions in two representative cases, i.e. $\theta = 271^\circ$ and 274°. For the first case ($\delta\eta = 4.7\%$), the row-averaged yaw angle decreases linearly from 28° in R1 to 0° in R10. Within a row, the yaw angle difference between columns is insignificant, which echoes well with the observations in section 5.2. As a result of this yaw angle distribution pattern, the wind turbines in the second and the last three rows produce less power than the rest rows. In the case of $\theta = 274^\circ$ ($\delta\eta = 15.7\%$, local peak), the optimal yaw angles for R1-R9 are roughly the same, pivoting around a median value of 14°. This yaw angle pattern leads to a rather uniform power production across the wind farm (expect for R1, which obviously delivers the highest power). A further check of the yaw angle and power distributions at the other peaks of $\delta\eta$ indicate the appearance of similar patterns. Recall the analysis in section 5.3 that the maximum power improvement is usually reached in the partial wake conditions, where a high spanwise velocity gradient is experienced by the downstream wind turbines. Actually, the spanwise extent of the high-velocity-gradient region is rather narrow. If a high yaw angle is applied and the resultant wake deflection exceeds this spanwise extent, the extra power gained by the downstream wind turbines is minimal. As a result, to maximize the overall power production of the wind farm at $\theta = 274^\circ$, a moderate yaw angle (wake deflection) should be sustained across the wind farm. In addition, it is interesting to note that the turbine located at the top-right corner yields more

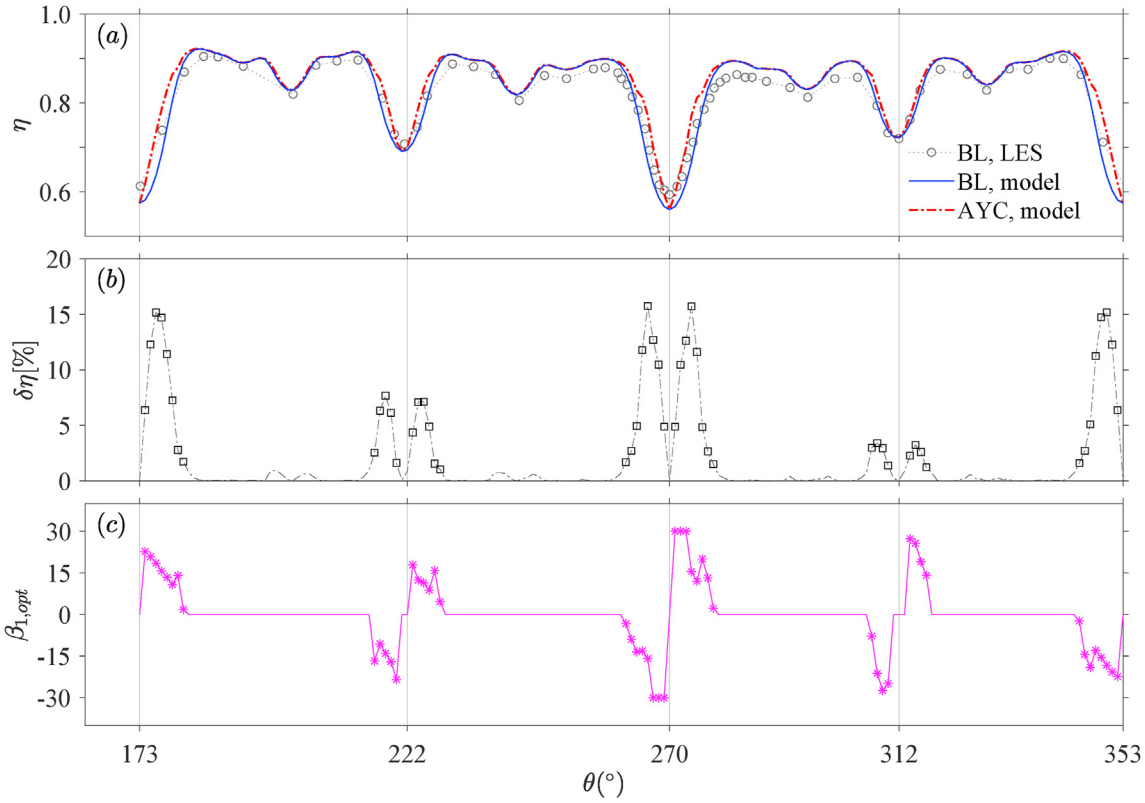

Fig. 17. (*a*) Impact of active yaw control on Horns-Rev wind farm efficiency. The baseline condition is abbreviated as BL in the legend. The LES data of the baseline wind farm efficiency is extracted digitally from Ref. [29]. (*b*) Relative power improvement at different wind directions. Symbols indicate the cases of $\delta\eta > 1$. (*c*) The optimal yaw angle of the leading wind turbine in the cases of $\delta\eta > 1$.

power than those in the same row, largely because at $\theta = 274^{\circ}$, half of its rotor disk is exposed directly to the free stream and suffered little from the wake effects.

7. Summary

In this study, wind tunnel experiments and analytical models are effectively combined to explore the full potential of active yaw control (AYC) in wind farm power optimization. In the experimental part, a three-row miniature wind farm with a fixed row spacing of 5*D* is constructed, and the power production and wake velocity fields of this wind farm are measured at various yaw angle distributions, for both full-wake and partial-wake conditions. Based on the physics learnt from the experiments (e.g. wake width variation, secondary wake steering effect), a new analytical wind farm model is developed, incorporating the recent progress in yawed wind turbine wakes and wake superposition principles. Using this analytical model, a parametric study of the effectiveness of AYC is pursued, covering the influence of the number of rows/columns, turbulence intensity and streamwise spacing. The main conclusions drawn from these analyses are recapped as follows.

Experimental results indicate that, regardless of the wake condition (full wake or partial wake), the optimal yaw angle distribution always exhibits a decreasing trend from upstream to downstream. This decreasing trend is rooted in the secondary wake steering effect. Specifically, due to the non-vanishing transverse velocity induced by an upstream yawed wind turbine, the wakes of the downstream wind turbines convect sidewards naturally, and thus less yawing is needed for them to achieve the same amount of wake deflection. The power map measured in the full-wake condition shows an approximate odd symmetry with respect to the yaw angle distribution, which together with the zero wake deflection exhibited by a wind turbine at zero yaw, justifies that positive and negative yaw are equally efficient in wake steering, at least for the neutral boundary layers investigated in this study. The relative power improvement in AYC varies noticeably with the spanwise offset between adjacent turbine rows, manifesting two maxima ($>15\%$) in the partial wake conditions and a local minimum (5.4%) in the full-wake condition. Particularly, when the spanwise offset exceeds 1*D*, the extra power earned by AYC becomes negligible. These variations can be explained from the different spanwise velocity gradients experienced by downstream wind turbines.

Parametric studies based on the analytical model show that, among all the parameters considered, the number of columns has the least influence on the effectiveness of AYC, which is due to the fact that the maximum wake deflection at infinity is a bounded value ($\approx 0.8D$) that is much smaller than the typical spacing between turbine columns. For a single-column wind farm operating in full-wake conditions, the relative power improvement ($\delta\eta$) increases asymptotically with the number of rows, as a result of the almost constant yaw angle distribution in the middle part of the wind farm. The optimal yaw angle of the leading wind turbine is limited by a critical yaw angle determined mainly by the cosine exponent of the thrust coefficient (p). For a typical value of $p = 1.8$, this critical yaw angle is approximately 30°. Turbulence intensity and streamwise spacing have similar impacts on the effectiveness of AYC, since both of them modify the strength of baseline wake interactions, and thus the margin in power optimization. As these two parameters increase, the relative value of $\delta\eta$ reduces monotonically. The peak location of $\delta\eta$ is only sensitive to the variation of turbulence intensity and roughly independent of the streamwise

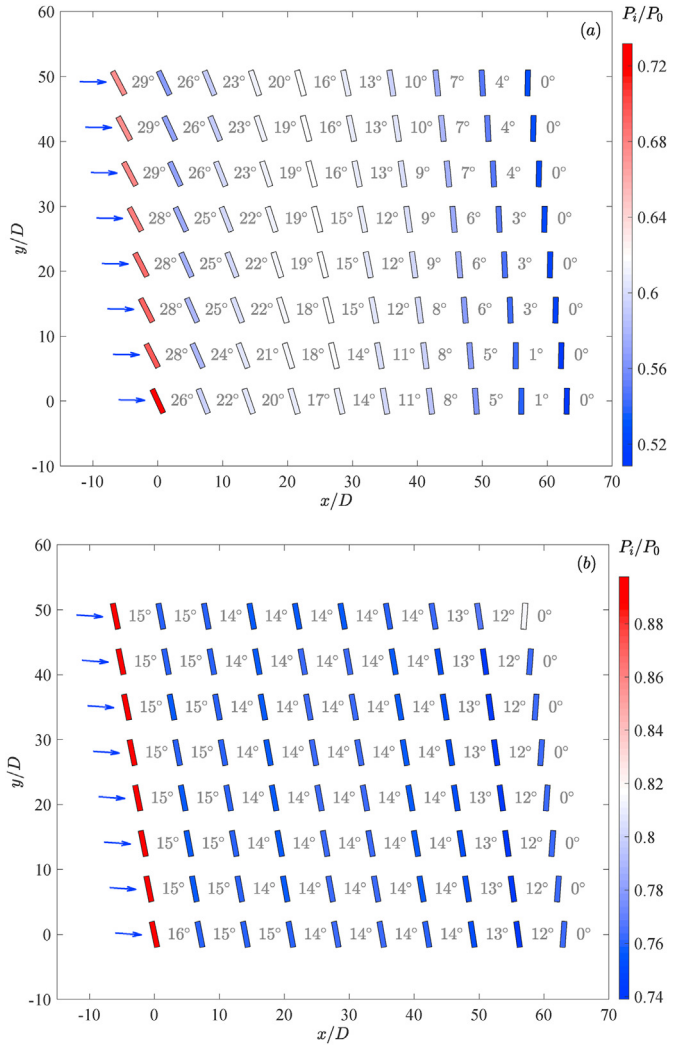

Fig. 18. Optimal yaw angle and power distributions in Horns-Rev wind farm at (*a*) $\theta = 271^\circ$ and (*b*) $\theta = 274^\circ$.

spacing.

In the last section of this study, the proposed model is further deployed to evaluate the potential of AYC in the Horns-Rev wind farm. At a typical turbulence level of 7.7% and wind speed of 8 m/s, significant power improvements up to 15.7% are achieved in the four wind sectors involving full-wake interactions within a streamwise distance of 10*D*. The relative variation of the annual wind farm efficiency is estimated to be 1.8%. For future studies, the variability of wind speed and direction should be taken into account during the power optimization process, and the impact of active yaw on the life spans of the major turbine components should be carefully evaluated.

CRediT authorship contribution statement

Fernando Porté-Agel: Conceptualization, Writing - review & editing, Funding acquisition, Resources.

Declaration of competing interest

The authors declare that they have no known competing financial interests or personal relationships that could have appeared to influence the work reported in this paper.

Acknowledgements

This research was funded by the Swiss National Science Foundation (grant number: 200021_172538) and the Swiss Federal Office of Energy (grant number: SI/502135-01). In addition, this project was carried out within the frame of the Swiss Centre for Competence in Energy Research on the Future Swiss Electrical Infrastructure (SCCER-FURIES) with the financial support of the Swiss Innovation Agency (Innosuisse—SCCER program, contract number: 1155002544.

References

[1] R.J. Stevens, C. Meneveau, Flow structure and turbulence in wind farms, Annu. Rev. Fluid Mech. 49 (2017).
[2] F. Porté-Agel, M. Bastankhah, S. Shamsoddin, Wind-turbine and wind-farm flows: a review, Boundary-Layer Meteorol. 174 (2020) 1–59.
[3] P.A. Fleming, P.M. Gebraad, S. Lee, J.W. van Wingerden, K. Johnson, M. Churchfield, J. Michalakes, P. Spalart, P. Moriarty, Evaluating techniques for redirecting turbine wakes using sowfa, Renew. Energy 70 (2014) 211–218.
[4] F. Campagnolo, V. Petrović, C.L. Bottasso, A. Croce, Wind tunnel testing of wake control strategies, in: 2016 American Control Conference (ACC), IEEE, 2016, pp. 513–518.
[5] M.F. Howland, J. Bossuyt, L.A. Martínez-Tossas, J. Meyers, C. Meneveau, Wake structure in actuator disk models of wind turbines in yaw under uniform inflow conditions, J. Renew. Sustain. Energy 8 (2016), 043301.
[6] S. Kanev, F. Savenije, W. Engels, Active wake control: an approach to optimize the lifetime operation of wind farms, Wind Energy 21 (2018) 488–501.
[7] P. Fleming, J. Annoni, J.J. Shah, L. Wang, S. Ananthan, Z. Zhang, K. Hutchings, P. Wang, W. Chen, L. Chen, Field test of wake steering at an offshore wind farm, Wind Energy Science 2 (2017) 229–239.
[8] P. Fleming, J. King, K. Dykes, E. Simley, J. Roadman, A. Scholbrock, P. Murphy, J.K. Lundquist, P. Moriarty, K. Fleming, et al., Initial results from a field campaign of wake steering applied at a commercial wind farm–part 1, Wind Energy Science 4 (2019) 273–285.
[9] M.F. Howland, S.K. Lele, J.O. Dabiri, Wind farm power optimization through wake steering, Proc. Natl. Acad. Sci. Unit. States Am. 116 (2019) 14495–14500.
[10] D. Medici, Experimental Studies of Wind Turbine Wakes: Power Optimisation and Meandering, Ph.D. thesis, KTH, 2005.
[11] M. Adaramola, P.Å. Krogstad, Experimental investigation of wake effects on wind turbine performance, Renew. Energy 36 (2011) 2078–2086.
[12] A. Ozbay, W. Tian, Z. Yang, H. Hu, Interference of wind turbines with different yaw angles of the upstream wind turbine, in: 42nd AIAA Fluid Dynamics Conference and Exhibit, 2012, p. 2719.
[13] M. Bastankhah, F. Porté-Agel, Wind farm power optimization via yaw angle control: a wind tunnel study, J. Renew. Sustain. Energy 11 (2019), 023301.
[14] J. Park, K.H. Law, Cooperative wind turbine control for maximizing wind farm power using sequential convex programming, Energy Convers. Manag. 101 (2015) 295–316.
[15] N.O. Jensen, A Note on Wind Generator Interaction, 1983.
[16] Á. Jiménez, A. Crespo, E. Migoya, Application of a les technique to characterize the wake deflection of a wind turbine in yaw, Wind Energy 13 (2010) 559–572.
[17] P.M. Gebraad, F. Teeuwisse, J. Van Wingerden, P.A. Fleming, S. Ruben, J. Marden, L. Pao, Wind plant power optimization through yaw control using a parametric model for wake effects–a cfd simulation study, Wind Energy 19 (2016) 95–114.
[18] L.A. Martínez-Tossas, J. Annoni, P.A. Fleming, M.J. Churchfield, The aerodynamics of the curled wake: a simplified model in view of flow control, Wind Energy Science 4 (1) (2019) 127–138.
[19] C. Bay, J. King, P. Fleming, R. Mudafort, L.A. Martínez-Tossas, Unlocking the Full Potential of Wake Steering: Implementation and Assessment of a Controls-Oriented Model. Technical Report, National Renewable Energy Lab.(NREL), Golden, CO (United States), 2019.
[20] M. Bastankhah, F. Porté-Agel, A new miniature wind turbine for wind tunnel experiments. part i: design and performance, Energies 10 (2017) 908.
[21] R.H. Dieck, Measurement Uncertainty: Methods and Applications, ISA, 2007.
[22] A. Sciacchitano, B. Wieneke, PIV uncertainty propagation, Meas. Sci. Technol. 27 (2016), 084006.
[23] R.J. Barthelmie, S.C. Pryor, S.T. Frandsen, K.S. Hansen, J. Schepers, K. Rados, W. Schlez, A. Neubert, L. Jensen, S. Neckelmann, Quantifying the impact of wind turbine wakes on power output at offshore wind farms, J. Atmos. Ocean. Technol. 27 (2010) 1302–1317.
[24] L. Vollmer, G. Steinfeld, D. Heinemann, M. Kühn, Estimating the wake deflection downstream of a wind turbine in different atmospheric stabilities: an LES study, Wind Energy Science 1 (2016) 129–141.
[25] M. Bastankhah, F. Porté-Agel, Experimental and theoretical study of wind turbine wakes in yawed conditions, J. Fluid Mech. 806 (2016) 506–541.
[26] P. Fleming, J. Annoni, M. Churchfield, L.A. Martinez-Tossas, K. Gruchalla, M. Lawson, P. Moriarty, A Simulation Study Demonstrating the Importance of Large-Scale Trailing Vortices in Wake Steering. Technical Report, National

Renewable Energy Lab.(NREL), Golden, CO (United States), 2018.
[27] I. Katic, J. Højstrup, N.O. Jensen, A simple model for cluster efficiency, in: European Wind Energy Association Conference and Exhibition, A. Raguzzi, 1987.
[28] A. Niayifar, F. Porté-Agel, Analytical modeling of wind farms: a new approach for power prediction, Energies 9 (2016) 741.
[29] F. Porté-Agel, Y.T. Wu, C.H. Chen, A numerical study of the effects of wind direction on turbine wakes and power losses in a large wind farm, Energies 6 (2013) 5297–5313.
[30] A. Crespo, J. Herna, et al., Turbulence characteristics in wind-turbine wakes, J. Wind Eng. Ind. Aerod. 61 (1996) 71–85.
[31] E. Bot, FarmFlow validation against full scale wind farms, Eur. Chem. News (2015).
[32] G.W. Qian, T. Ishihara, A new analytical wake model for yawed wind turbines, Energies 11 (2018) 665.
[33] M. Bastankhah, F. Porté-Agel, A new analytical model for wind-turbine wakes, Renew. Energy 70 (2014) 116–123.
[34] C.R. Shapiro, D.F. Gayme, C. Meneveau, Modelling yawed wind turbine wakes: a lifting line approach, J. Fluid Mech. 841 (2018).
[35] P. Vermeulen, An experimental analysis of wind turbine wakes, in: 3rd International Symposium on Wind Energy Systems, 1980, pp. 431–450.
[36] F. Carbajo Fuertes, C. Markfort, F. Porté-Agel, Wind turbine wake characterization with nacelle-mounted wind lidars for analytical wake model validation, Rem. Sens. 10 (2018) 668.
[37] H. Zong, F. Porté-Agel, A momentum-conserving wake superposition method for wind farm power prediction, J. Fluid Mech. 889 (2020) A8.
[38] S.B. Pope, Turbulent Flows, 2001.